Journal of Sustainable Metallurgy (2023) 9:1253–1266
https://doi.org/10.1007/s40831-023-00727-9

RESEARCH ARTICLE

Chlorination of $ZnFe_2O_4$ by Molten $MgCl_2$: Effect of Adding $CaCl_2$

Jingdong Huang[1,2] · **Guangqiang Li**[3] · **Xiao Yang**[2]

Received: 9 March 2023 / Accepted: 28 July 2023 / Published online: 9 August 2023
© The Minerals, Metals & Materials Society 2023, corrected publication 2023

Abstract

Natural Zn reserves might be exhausted in the following decades. Electric arc furnace (EAF) dust is an essential secondary Zn resource. The recovery of Zn from EAF dust is a critical factor in the sustainable development of the Zn industry and steelmaking industry. Efficient destruction of the $ZnFe_2O_4$ crystal structure and separation of Zn and Fe are the key issues to recycle EAF dust. Molten metal chlorides are believed to be effective in breaking the structure of $ZnFe_2O_4$. This work clarifies the distinct reaction behavior between $ZnFe_2O_4$ and $MgCl_2$ or $CaCl_2$. Experiments show that although $MgCl_2$ is a more powerful chlorinating agent, the capability of separating Zn and Fe is not as good as that of $CaCl_2$. Fast and selective chlorination of Zn from $ZnFe_2O_4$ happens by reacting $ZnFe_2O_4$ and $MgCl_2$–$CaCl_2$ mixture. $CaCl_2$ facilitates the formation of stable Fe-bearing phases, such as $MgFe_2O_4$ and $Ca_2Fe_2O_5$, thereby inhibiting the chlorination of Fe. Moreover, it becomes more effective in promoting the selectivity of chlorinating Zn by increasing temperature after adding $CaCl_2$ in $MgCl_2$. When $ZnFe_2O_4$ is subjected to chlorination using a $MgCl_2$–$CaCl_2$ mixture ($MgCl_2$–$CaCl_2$–$ZnFe_2O_4$ molar ratio = 1.5:1.5:1) at 950 °C for 120 min, the process results in a chlorination percentage of over 90% for Zn, with Fe chlorination percentage lower than 5%. These results demonstrate the prospect of efficient separation of Zn from $ZnFe_2O_4$ by reaction with molten $MgCl_2$–$CaCl_2$ mixture.

Graphical Abstract

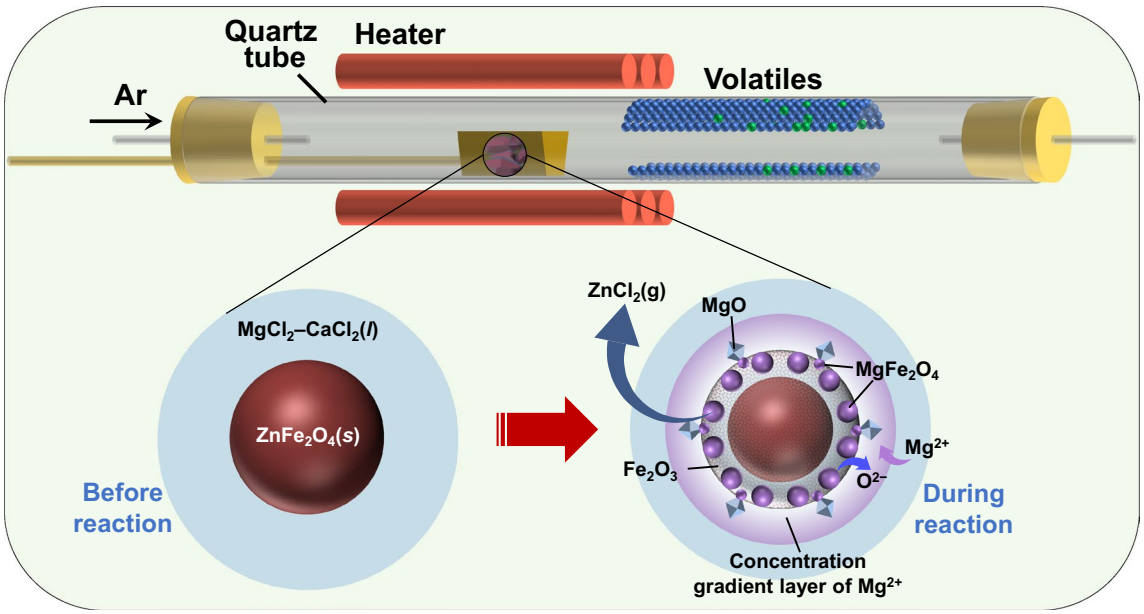

Keywords Zinc ferrite · Chlorination · Magnesium chloride · Calcium chloride · Electric arc furnace dust

The contributing editor for this article was Hongmin Zhu.

Extended author information available on the last page of the article

Introduction

Zn is an essential element for modern society. The steel industry is the largest consumer of Zn. In 2019, the quantity of Zn used for galvanizing steel was 10,167 kt, which represented over 50% of the global Zn production [1]. Coating a thin Zn layer on the steel surface is a simple and efficient way to protect the base metal from corrosion and rusting. Galvanized steel is thus among the most popular steel types and is widely applied in various industrial sectors. When scrap steel is remelted in an electric arc furnace (EAF), all Zn evaporates and gets into the EAF dust. In these cases, the Zn content in EAF dust varies from 5 to 40% [2]. Figure 1 shows the schematic illustration of the mass flow of Zn in the steel industry. Complete recycling of Zn from EAF dust would increase the circularity of Zn and reduce the dependence on natural resources. However, the actual situation is that a large portion of EAF dust (around 37%) is sent to landfills because of the technical difficulties in recycling. Rostek et al. estimated that the loss of Zn in the steel industry was 500 kt in 2019 [1]. On the other hand, Zn is recognized as one of the elements with limited natural supplies. The US Geological Survey's latest report suggested that the Zn mine might be exhausted within 20 years [3]. Due to the value of Zn and the gradual depletion of natural reserves, boosting the recycling ratio of Zn from EAF dust has become a vital issue in Zn sustainability.

$ZnFe_2O_4$, ZnO, and Fe_2O_3 are the main components in EAF dust. The difficulty in recovering Zn from EAF dust is because of the high chemical stability of $ZnFe_2O_4$ [4, 5]. Both pyrometallurgical and hydrometallurgical techniques can treat EAF dust [6–14]. Pyrometallurgy is the primary choice due to the high metal recovery ratio and relatively short process [15]. The Waelz process and the rotary hearth furnace technology are two typical routes with commercial applications. Both are based on carbothermic reduction at high temperatures [16]. The Zn-bearing oxides in the dust are reduced by coke at around 1200 °C to form Zn vapor, which is later re-oxidized by air to ZnO. The final recycled product is crude ZnO powder instead of metallic Zn. However, high-energy consumption and massive emission of CO_2 are the main drawbacks, especially as the goal of achieving carbon neutrality has become an international consensus. Therefore, innovations in Zn recycling from EAF dust are urgently needed. Recently, Nagasaka et al. proposed a "CaO addition process" to replace the Waelz process after years of fundamental and systematic research input [17]. In this technology, EAF dust is mixed with CaO at a high temperature (e.g., 1000 °C). CaO would react with $ZnFe_2O_4$ in the dust to form ZnO and $Ca_2Fe_2O_5$. Because ZnO is far easier to dissolve than $ZnFe_2O_4$ in acid or alkali solutions, metallic Zn can be obtained after leaching and electrolysis [18, 19]. The most significant advantage of this technology is that carbothermic reduction is no longer necessary. However, the slow solid-state reaction between dust and CaO remains a challenge for industrial applications.

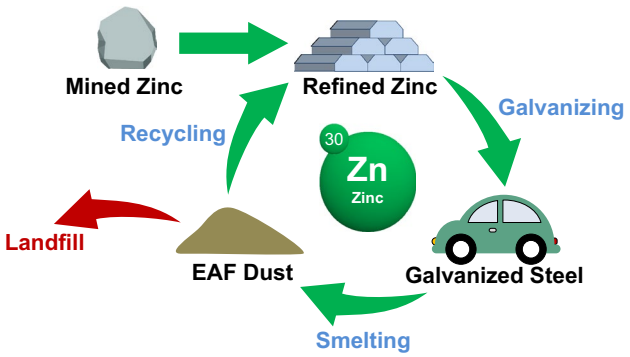

Fig. 1 Schematic of the mass flow of Zn in steel industry

Chlorination-based pyrometallurgical processes have significant advantages in terms of efficiency and low carbon emissions [20–25]. Zn-bearing oxides can be converted into $ZnCl_2$ by Cl_2, polyvinyl chloride (PVC), or metal chlorides through a rapid gas–solid or liquid–solid reaction. Metallic Zn can be easily obtained by electrolyzing molten $ZnCl_2$. In principle, no carbon-based reducing agent is required for the chlorination process. Matsuura et al. [26–28] carried out systematic research on using Cl_2 as the chlorinating agent. As reported, Zn in EAF dust could be efficiently and selectively chlorinated utilizing a mixture of Cl_2 and O_2. However, the high corrosiveness and toxicity of Cl_2 pose challenges to equipment corrosion and safety issues. Finding a Cl_2-free substance as the chlorinating agent to make the process easier and safer is necessary. Apart from Cl_2, PVC has been utilized as a functional chlorinating additive to assess the feasibility of recycling EAF dust for metal extraction [29–34]. By reacting EAF dust with PVC, Zn in EAF dust is converted to $ZnCl_2$ by hydrogen chloride (HCl) gas evolved from PVC. However, generating dioxin and other pollutants from PVC at high temperatures is a disadvantage.

Molten metal chlorides can also be used as chlorinating agents in place of Cl_2 and PVC. Guo et al. clarified that molten $CaCl_2$ converts Zn in $ZnFe_2O_4$ into gaseous $ZnCl_2$ while making Fe remain in the solid residue as $CaFe_2O_4$ [35–38]. This result indicates a high selectivity of chlorinating Zn by $CaCl_2$. However, the sluggish reaction is not satisfied from a practical standpoint. Since $MgCl_2$ is another common chloride with higher reactivity to chlorinate solid oxides [39, 40], we propose an alternative technology of using $MgCl_2$ to treat EAF dust. The target product is $ZnCl_2$. Previously, we demonstrated the capability of $MgCl_2$ to chlorinate $ZnFe_2O_4$ [41]. $MgCl_2$ converts Zn in $ZnFe_2O_4$ to $ZnCl_2$ more efficiently than $CaCl_2$. Reaction temperature could be lower, and the rate

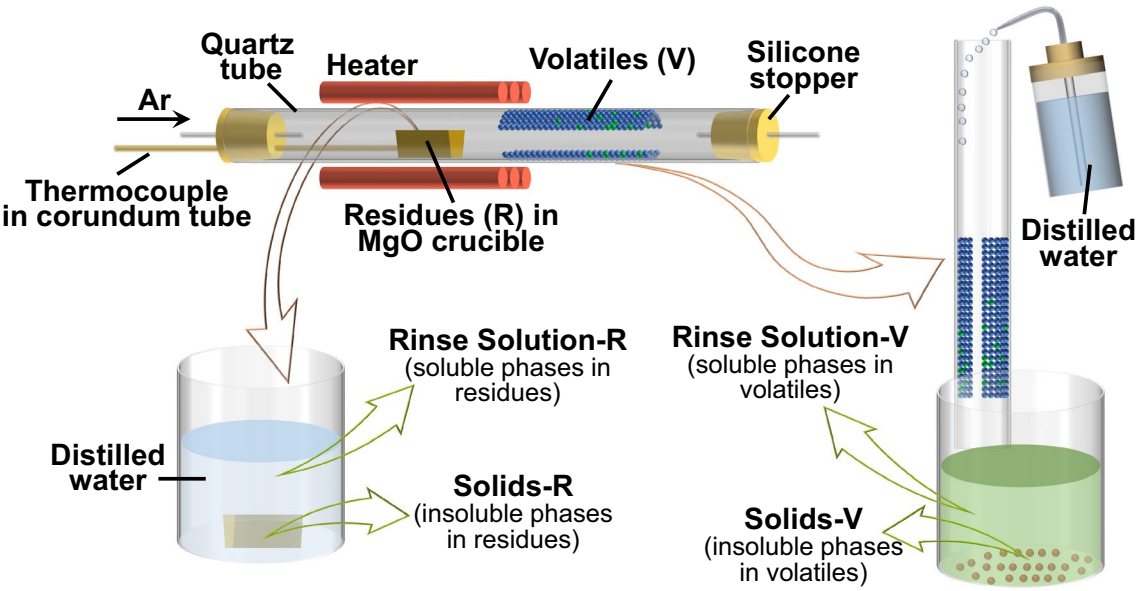

Fig. 2 Schematic diagram of the experimental setup and post-treatment process for products analysis

is larger when using $MgCl_2$. However, a part of Fe in $ZnFe_2O_4$ is also chlorinated to form volatile iron chlorides, which means $MgCl_2$ is not as good as $CaCl_2$ in terms of selective chlorination of Zn.

Considering the distinct features of $MgCl_2$ and $CaCl_2$, using $MgCl_2$ with the addition of $CaCl_2$ may lead to fast and selective chlorination of Zn from $ZnFe_2O_4$. This work compares the chlorination behaviors of $ZnFe_2O_4$ between using $MgCl_2$ and using $CaCl_2$ and demonstrates the superior efficacy of using the $MgCl_2$–$CaCl_2$ mixture. The reaction mechanism and the effects of thermodynamic conditions (mixture composition, temperature, etc.) on the chlorination behaviors of Zn and Fe are clarified. This work may optimize the technology based on utilizing chlorides for Zn recovery from EAF dust.

Materials and Method

Materials

Reagent grade ZnO (99%, Aladdin), Fe_2O_3 (99%, Aladdin), $MgCl_2$ (99%, Aladdin), and $CaCl_2$ (97%, Aladdin) were used. ZnO and Fe_2O_3 (molar ratio of 1:1) were thoroughly mixed and sintered in air at 1100 °C for 24 h to prepare $ZnFe_2O_4$. The as-prepared $ZnFe_2O_4$ was ground, and particles in size range from 0.10 mm to 0.28 mm were used in the experiments. All chemicals were vacuum dried at 200 °C for at least 24 h before use.

Experimental Procedure

The experiment was performed in a horizontal tube furnace, as shown in Fig. 2. A MgO crucible (cuboid shape, length 60 mm, width 30 mm, depth 20 mm) containing a powdery sample was set in a quartz tube in the furnace. The samples were a mixture of $MgCl_2$ and $ZnFe_2O_4$ (0.2856 g and 0.2410 g, molar ratio = 3:1), a mixture of $CaCl_2$ and $ZnFe_2O_4$ (0.3329 g and 0.2410 g, molar ratio = 3:1), and mixtures of $MgCl_2$, $CaCl_2$, and $ZnFe_2O_4$ with different molar ratios. High-purity Ar was introduced as the protective gas at 200 mL min^{-1}. The reaction temperature was from 800 °C to 1000 °C.

The weight loss of the sample during the reaction was measured. As shown in Fig. 2, a corundum tube enclosing a thermocouple was placed inside the quartz tube, ensuring that the tube tip was at the center (hot zone). Once the furnace temperature reached the desired value, the reactant-filled MgO crucible was moved from the cold zone to the hot zone within the quartz tube. After a specific duration, the corundum tube was quickly pushed to return the crucible back to the quartz tube end (cold zone). The crucible was then retrieved using a stainless-steel clamp and weighed. To prevent the direct contact between the hot crucible and the balance, a quartz crucible was placed on the balance. After weighing, the crucible was placed back in the quartz tube center. These steps were repeated multiple times to plot the weight loss curve.

During reaction, volatiles would form, evaporate, and deposit on the inner quartz wall in the cold zone, while solid residues should remain in the crucible. In some cases,

quartz wools were set in the quartz tube to collect the volatiles. After reaction, the quartz tube was rinsed with distilled water to dissolve the volatiles deposited on the inner wall. The crucible was also rinsed by immersing it in distilled water. Accordingly, substances after reaction were divided into four parts (Fig. 2): Rinse Solution-V (containing soluble phases in volatiles denoted by V) and Solids-V (insoluble phases in volatiles) from volatiles, Rinse Solution-R (containing soluble phases in residues in crucible denoted by R) and Solids-R (insoluble phases in residues in crucible) from the residues in crucible. These four parts of substances were analyzed by phase or chemical analysis, respectively.

Analysis and Characterization

Phase compositions of Solids-V and Solids-R were analyzed by an X-ray diffractometer (XRD, Cu K_{α}, 40 kV, 40 mA, 5° min^{-1}, Bruker, D8 Advance). When using quartz wools to collect volatiles, the quartz wools were ground into powder in a glove box after the reaction. The powdery sample was also analyzed by XRD. In addition, the microstructures of Solids-V and Solids-R were observed by a scanning electron microscope (SEM, Zeiss Gemini 450) equipped with an energy-dispersive spectrometer (EDS, Oxford instrument). Raman spectra were recorded on a spectrometer (WITec, Alpha300R) using a laser source with an excitation wavelength of 532 nm in the range of 100–900 cm^{-1}. Rinse Solution-V and Rinse Solution-R were subject to chemical analysis by an inductively coupled plasma mass spectrometer (ICP – MS, ThermoFisher, iCAP RQ). The fractions of Zn and Fe (F_M) in Rinse Solution-V and Rinse Solution-R can be calculated by

$$F_M(\%) = \frac{C_M \times V}{W_M} \times 100\% \quad (1)$$

where C_M is the concentration of a metal ion in the solution (g L^{-1}), V is the total volume of the solution (L), and W_M is the total mass of Zn or Fe in initial $ZnFe_2O_4$. Although deposits on the quartz tube wall may contain water-insoluble FeOCl that is difficult to recover completely [41], this phase was formed in tiny quantities. Therefore, the sum of the fractions of Zn or Fe in Rinse Solution-V and Rinse Solution-R is defined as the chlorination percentage.

Results and Discussion

Distinct Reaction Behavior of $ZnFe_2O_4$ Between Using $MgCl_2$ and Using $CaCl_2$

Based on our previous experiments, when the molar ratio of $MgCl_2$ to $ZnFe_2O_4$ was 1:1, only less than 50% of Zn in

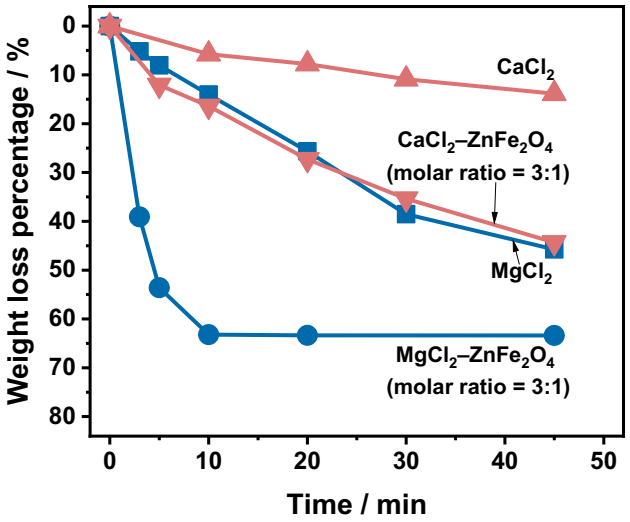

Fig. 3 Weight loss percentage curves of different samples [$MgCl_2$ (0.2856 g), $CaCl_2$ (0.3330 g), $MgCl_2$–$ZnFe_2O_4$ mixture (0.2856 g–0.2410 g; molar ratio = 3:1) and $CaCl_2$–$ZnFe_2O_4$ mixture (0.3330 g–0.2410 g; molar ratio = 3:1)] at 950 °C in Ar

$ZnFe_2O_4$ was chlorinated [41]. Therefore, a molar ratio of 3:1 was adopted to ensure sufficient chlorination of Zn in this work. Figure 3 shows the weight loss percentage curves of pure chlorides and chloride-oxide mixtures at 950 °C in Ar. The weight loss rate of chloride/oxide mixtures is more significant than their corresponding pure chlorides, suggesting the chlorination of $ZnFe_2O_4$ by $MgCl_2$ or $CaCl_2$ to form volatiles. The weight of $MgCl_2$–$ZnFe_2O_4$ mixture decreases rapidly and reaches a constant value within 10 min, while the weight loss of $CaCl_2$–$ZnFe_2O_4$ mixture is much slower. The result confirms that $MgCl_2$ is more potent in chlorination compared with $CaCl_2$.

Figure 4a shows the variation of chlorination percentage of Zn and Fe for the $MgCl_2$–$ZnFe_2O_4$ and $CaCl_2$–$ZnFe_2O_4$ mixtures (molar ratio = 3:1 for both cases) at 950 °C in Ar. According to the increasing rate of chlorination percentage, chlorination of Zn is faster than that of Fe in both cases, suggesting the preference for chlorinating Zn over Fe. In the case of using $MgCl_2$, chlorination of Zn shows a tendency of "fast followed by slow," while chlorination of Fe is "slow followed by fast." As a result, the molar ratio of Zn to Fe in Rinse Solution-V (the solution after rinsing volatiles with water) is gradually declining (Fig. 4b). In the case of using $CaCl_2$, chlorination of Zn is slower, and it seems like that Fe is rarely chlorinated. Accordingly, a continuous increase in the molar ratio of Zn to Fe in Rinse Solution-V can be noticed. The ratio reaches more than 100 after reaction for 10 min, which is far larger than the values of using $MgCl_2$. These results confirm that although $MgCl_2$ is a potent chlorinating agent, the capability of separating Zn and Fe is not as good as that of $CaCl_2$.

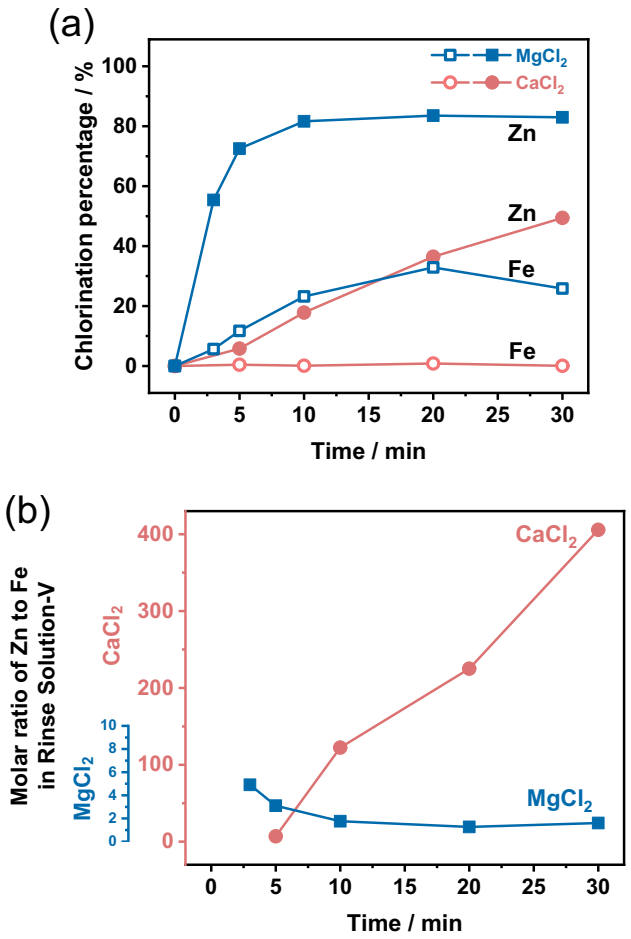

Fig. 4 Variation of **a** chlorination percentages of Zn and Fe and **b** molar ratios of Zn to Fe in Rinse Solution-V (containing soluble phases in volatiles) during the reactions between $ZnFe_2O_4$ and $MgCl_2$ or $CaCl_2$ (molar ratio = 3:1 for both cases) at 950 °C in Ar

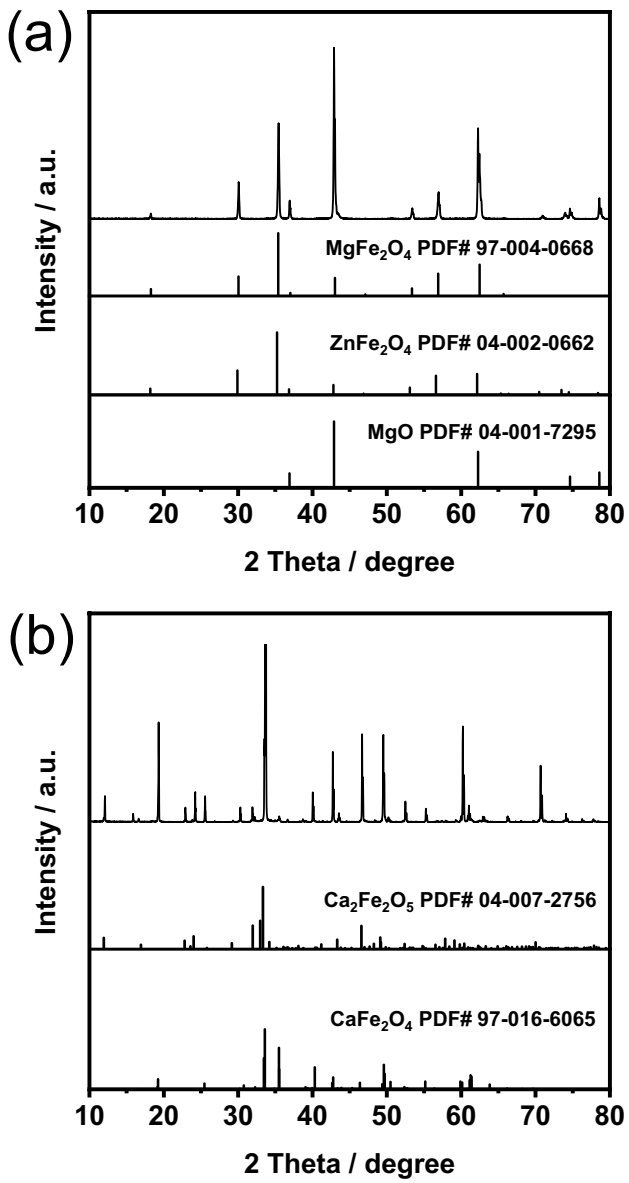

Fig. 5 XRD patterns of Solids-R (insoluble phases in residues in the crucible) after reacting $ZnFe_2O_4$ with **a** $MgCl_2$ and **b** $CaCl_2$ (molar ratio = 3:1) for 120 min at 950 °C in Ar

Figure 5 shows the XRD patterns of Solids-R (insoluble phases in residues in the crucible) after reacting $ZnFe_2O_4$ with $MgCl_2$ or $CaCl_2$ at 950 °C for 120 min. When reacting with $MgCl_2$, a spinel phase and MgO were detected. The spinel phase may be incompletely reacted $ZnFe_2O_4$ and newly formed $MgFe_2O_4$. When reacting with $CaCl_2$, $CaFe_2O_4$ and $Ca_2Fe_2O_5$ were detected. $ZnFe_2O_4$ should also remain in the $CaCl_2$ system. However, the presence of products such as $CaFe_2O_4$ and $Ca_2Fe_2O_5$ may envelop the remaining $ZnFe_2O_4$, making it challenging to detect through XRD. Figure 6 shows the SEM images and EDS mapping results of Solids-R in both cases. Fine particles can be observed in the products of the reaction between $ZnFe_2O_4$ and $MgCl_2$. EDS mapping indicates high concentrations of Mg and O while low concentrations of other elements in these particles (Fig. 6a). Although a small amount of $MgFe_2O_4$ forms, most of the solid phase products are MgO. In the case of reacting with $CaCl_2$, strips several hundred microns long can be detected. They were identified as $Ca_2Fe_2O_5$ (Fig. 6b). These observations are consistent with the previous findings of Guo et al. [37, 38].

We have clarified the reaction behavior between solid $ZnFe_2O_4$ and molten $MgCl_2$ in a previous work [41]. The chlorination of Zn is with higher priority

$$MgCl_2(l) + ZnFe_2O_4(s) \rightarrow MgO(s) + Fe_2O_3(s) + ZnCl_2(g) \quad (2)$$

Although the priority is lower, the chlorination of Fe also occurs

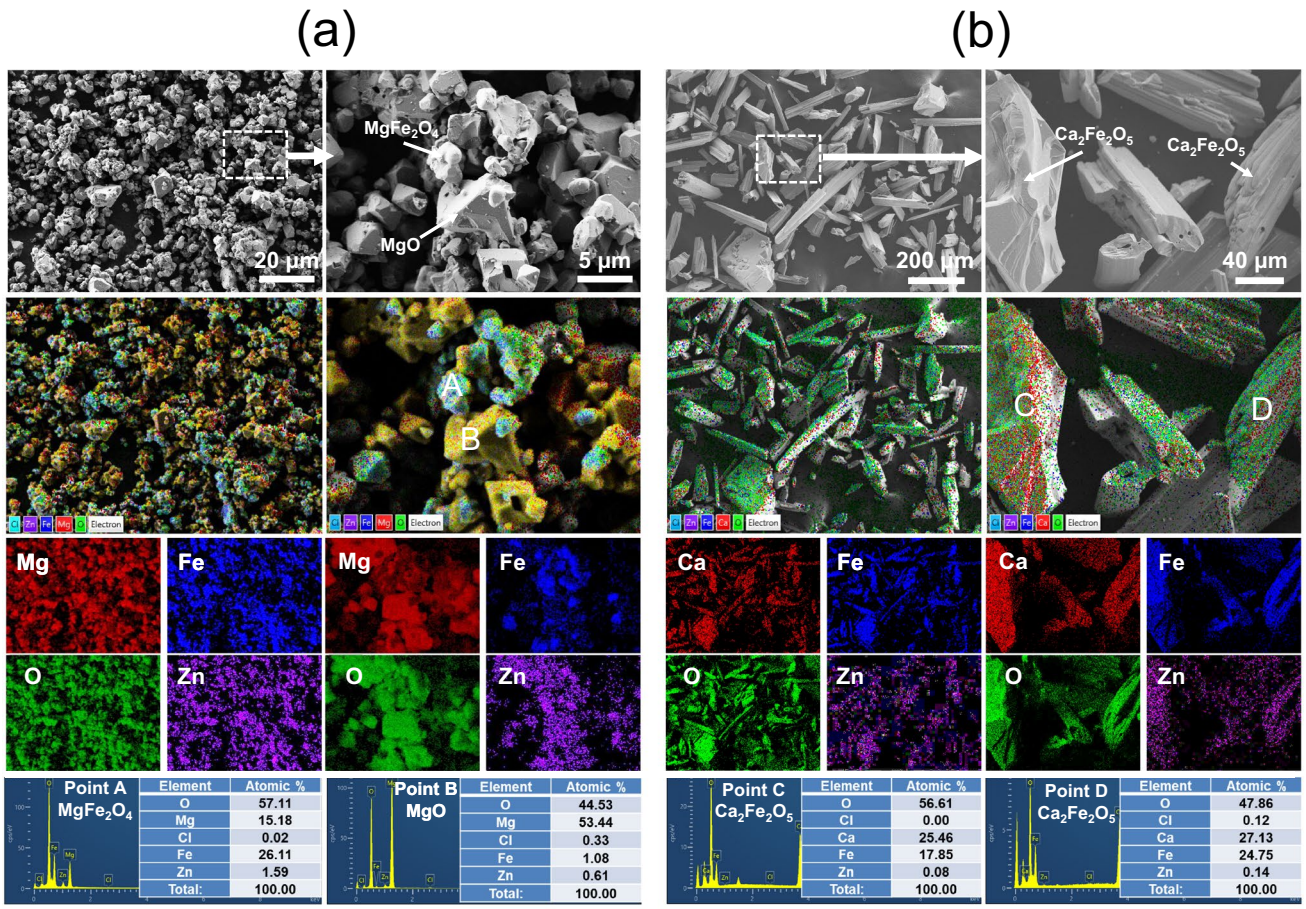

Fig. 6 SEM images and EDS mapping results of Solids-R (insoluble phases in residues in the crucible) after reacting $ZnFe_2O_4$ with **a** $MgCl_2$ and **b** $CaCl_2$ (molar ratio = 3:1) for 120 min at 950 °C in Ar

$$3MgCl_2(l) + Fe_2O_3(s) \rightarrow 3MgO(s) + 2FeCl_3(g) \quad (3)$$

In the case of reacting with $CaCl_2$, a similar reaction will occur

$$CaCl_2(l) + ZnFe_2O_4(s) \rightarrow CaO(s) + Fe_2O_3(s) + ZnCl_2(g) \quad (4)$$

$$\Delta_r G^0_{950\,^\circ C} = 87.24\ \text{kJ mol}^{-1}$$

Although reaction (4) is not spontaneous at standard state conditions, deviation from the standard state of products (CaO and $ZnCl_2$) may cause the reaction to proceed forward. Figure 7 shows the pH of the water-rinsed solutions of Solids-R. The increase in the pH after reacting with $CaCl_2$ is due to hydration of newly formed CaO, while the decrease in the pH after reacting with $MgCl_2$ is due to the hydration of MgO.

The dissolution behavior of CaO in molten $CaCl_2$ and that of MgO in molten $MgCl_2$ are rather different, which might be the primary reason for the dissimilar performances in separating Zn and Fe between the two chlorides. Because

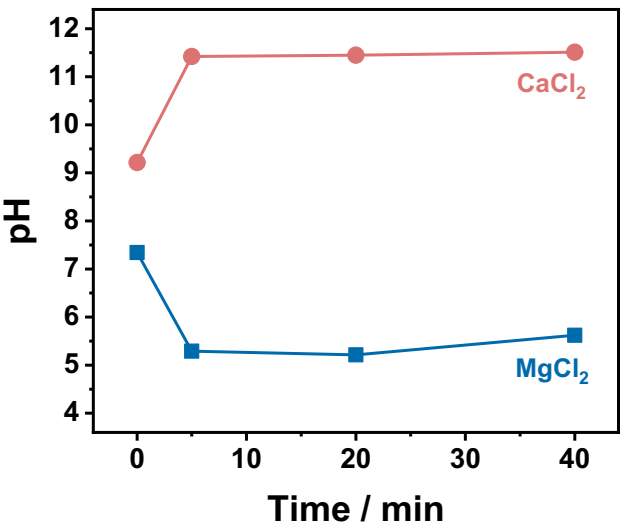

Fig. 7 The pH of the water-rinsed solutions of Solids-R after reacting $ZnFe_2O_4$ with $MgCl_2$ or $CaCl_2$ (molar ratio = 3:1) at 950 °C in Ar

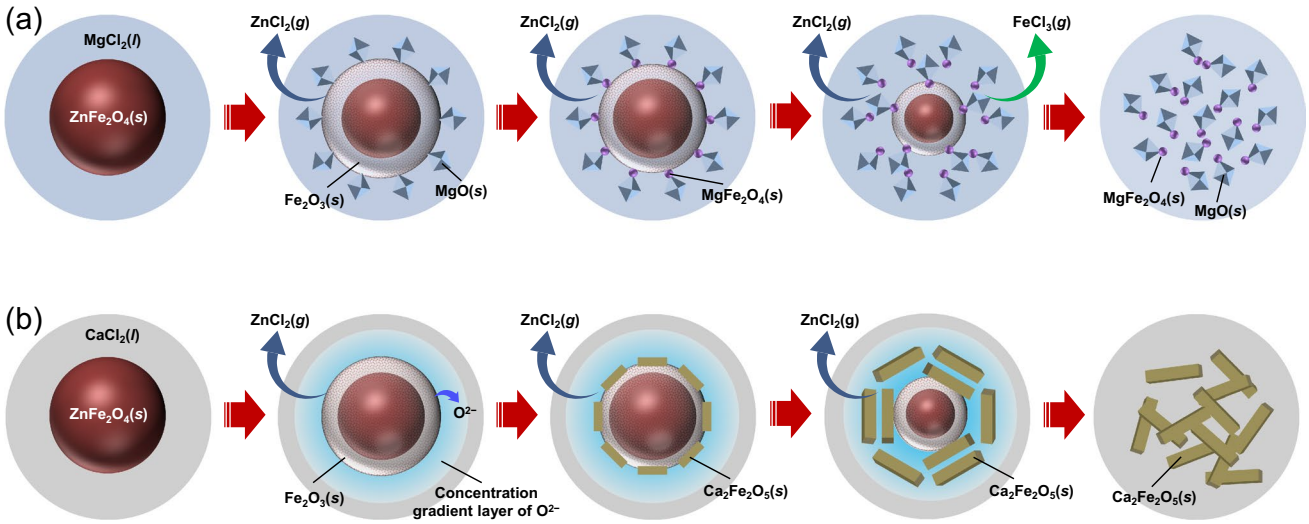

Fig. 8 Schematic representation of the reaction mechanisms between solid $ZnFe_2O_4$and **a** molten $MgCl_2$ or **b** molten $CaCl_2$

CaO is highly soluble and dissociable in molten $CaCl_2$ (solubility > 20 mol% at 950 °C [42]), CaO formed in reaction (4) will immediately dissociate into Ca^{2+} and O^{2-} in molten $CaCl_2$ and react with Fe_2O_3 to form new compounds by

$$CaO(s) \rightarrow Ca^{2+} + O^{2-} \tag{5}$$

$$Ca^{2+} + O^{2-} + Fe_2O_3(s) \rightarrow CaFe_2O_4(s) \tag{6}$$

$$2Ca^{2+} + 2O^{2-} + Fe_2O_3(s) \rightarrow Ca_2Fe_2O_5(s) \tag{7}$$

$CaFe_2O_4$ and $Ca_2Fe_2O_5$ are more stable than Fe_2O_3 [43], and thus, the chlorination of Fe is inhibited.

In contrast, $O.^{2-}$ is almost insoluble in molten $MgCl_2$ [44]. Although the following reactions may turn Fe_2O_3 into more stable $MgFe_2O_4$

$$Mg^{2+} + O^{2-} + Fe_2O_3(s) \rightarrow MgFe_2O_4(s) \tag{8}$$

$$MgO(s) + Fe_2O_3(s) \rightarrow MgFe_2O_4(s) \tag{9}$$

, the reaction rates must be low due to the low concentration of O^{2-} or limited surface area for reaction. As evidenced by the experimental results (Fig. 6), there was only a tiny amount of $MgFe_2O_4$ in Solids-R after reacting $ZnFe_2O_4$ with $MgCl_2$, and the particle size is far smaller than that of $Ca_2Fe_2O_5$ in the case of using $CaCl_2$. As a result, a considerable part of Fe was chlorinated to $FeCl_3$ when using $MgCl_2$.

Therefore, the mechanisms of chlorinating $ZnFe_2O_4$ by $MgCl_2$ and $CaCl_2$ can be summarized, as illustrated in Fig. 8. When $MgCl_2$ is used as the chlorinating agent, Zn in the lattice of $ZnFe_2O_4$ is first chlorinated to form $ZnCl_2$, MgO, and Fe_2O_3 [reaction (2)]. The newly formed MgO and Fe_2O_3 in contact with each other would react to produce a tiny amount of $MgFe_2O_4$. As Zn gets consumed, $MgCl_2$ gradually reacts with Fe_2O_3 to form $FeCl_3$ [reaction (3)]. Both $ZnCl_2$ and $FeCl_3$ leave the melt as volatiles soon after their formation. The final products remaining in the system as solid residues are MgO and $MgFe_2O_4$. In the case of using $CaCl_2$, after the reaction between $CaCl_2$ and $ZnFe_2O_4$ [reaction (4)], the newly formed CaO immediately dissolves in the melt and dissociates into mobile O^{2-}. A concentration gradient layer of O^{2-} from the interface to the bulk will form. The melt film surrounding the newly formed Fe_2O_3 will instantly become rich in O^{2-}, which turns the surface of Fe_2O_3 into more stable compounds such as $Ca_2Fe_2O_5$ and inhibits the further chlorination of Fe [reactions (5)–(7)]. $Ca_2Fe_2O_5$ is the major solid phase remaining in the system after sufficient reaction.

These findings suggest that the superior performance of $CaCl_2$ in separating Zn from Fe is because of the highly soluble and mobile nature of O^{2-} in molten $CaCl_2$. Therefore, we consider that adding $CaCl_2$ in $MgCl_2$ may promote the mobility of O^{2-} in the melt and thus achieve fast and selective separation of Zn from $ZnFe_2O_4$.

Chlorination of $ZnFe_2O_4$ by $MgCl_2$–$CaCl_2$

Figure 9 shows the chlorination percentages of Zn and Fe and molar ratios of Zn to Fe in Rinse Solution-V after the reactions between $ZnFe_2O_4$ and different $MgCl_2$–$CaCl_2$ mixtures at 950 °C for 120 min in Ar. The chlorination percentages of Fe decline clearly with the increase of $CaCl_2$ addition. The result demonstrates that adding $CaCl_2$ can enhance the selectivity of chlorinating Zn. Figure 10 shows the variation of chlorination percentages of Zn and Fe during the reactions between $ZnFe_2O_4$ and different $MgCl_2$–$CaCl_2$

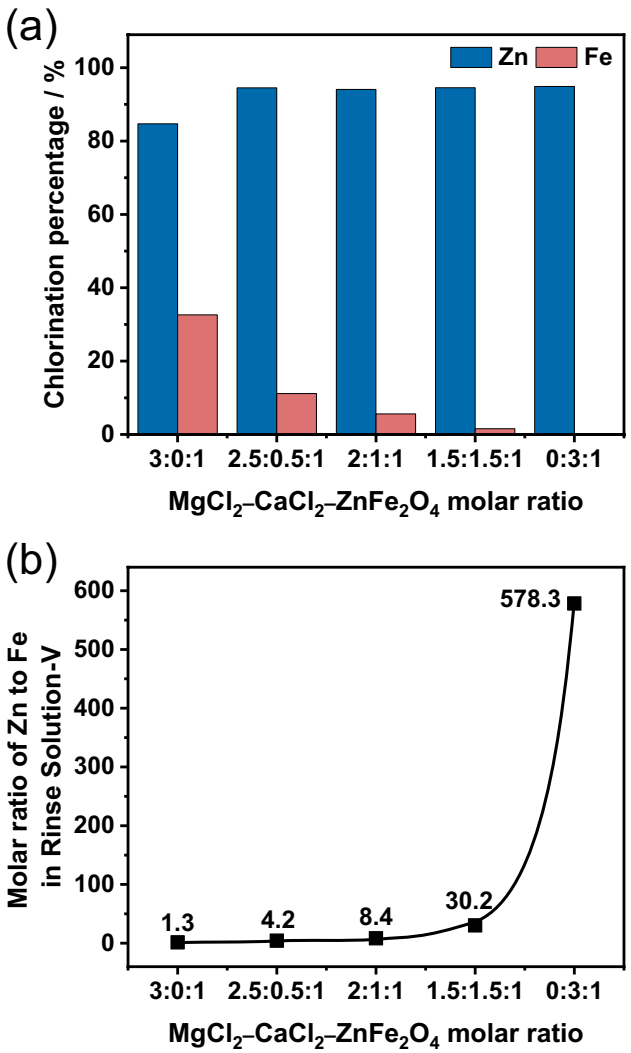

Fig. 9 **a** Chlorination percentages of Zn and Fe and **b** molar ratios of Zn to Fe in Rinse Solution-V (containing soluble phases in the volatiles) after the reactions between $ZnFe_2O_4$ and different $MgCl_2$–$CaCl_2$ mixtures at 950 °C for 120 min in Ar

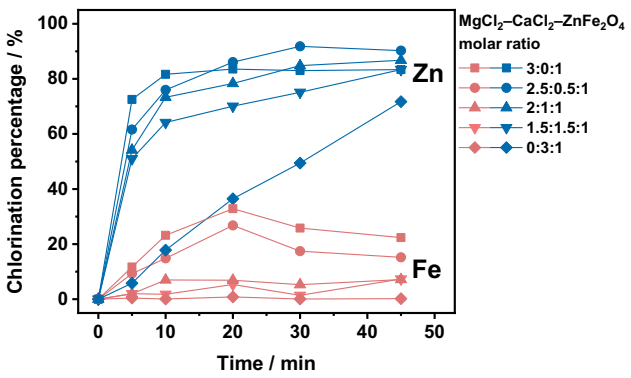

Fig. 10 Variation of chlorination percentages of Zn and Fe during the reactions between $ZnFe_2O_4$ and different $MgCl_2$–$CaCl_2$ mixtures at 950 °C in Ar

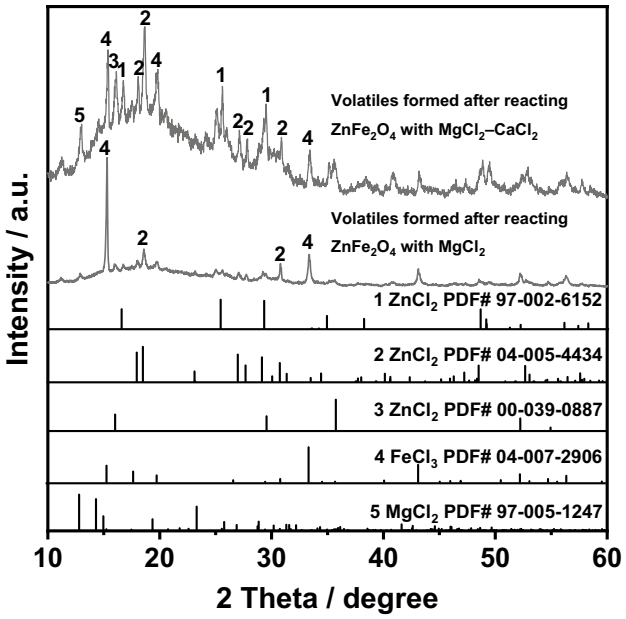

Fig. 11 XRD patterns of the volatiles formed after reacting $ZnFe_2O_4$ with $MgCl_2$ ($MgCl_2$–$ZnFe_2O_4$ molar ratio = 3:1) and $MgCl_2$–$CaCl_2$ mixture ($MgCl_2$–$CaCl_2$–$ZnFe_2O_4$ molar ratio = 2.5:0.5:1) at 950 °C for 45 min in Ar

mixtures at 950 °C in Ar. A decrease in chlorination rate with the increase in $CaCl_2$ addition can be noticed. It is considered that $MgCl_2$ plays the role of fast chlorination. $CaCl_2$ can inhibit the chlorination of Fe, yet it may slow down the overall reaction. There must be an optimum composition of the $MgCl_2$–$CaCl_2$ mixture to achieve the best chlorinating performance by balancing these two effects. It appears that the mixture of $MgCl_2$–$CaCl_2$ = 1:1 performs better than the others.

Volatiles formed during the reaction between $ZnFe_2O_4$ and $MgCl_2$–$CaCl_2$ mixture or $MgCl_2$ were collected and characterized by XRD, as shown in Fig. 11. Due to the addition of $CaCl_2$, the diffraction peaks of $FeCl_3$ are obviously weakened, consistent with the chemical analysis results that the addition of $CaCl_2$ lowers the chlorination percentage of Fe (Fig. 10).

As shown in Fig. 12, both the mass and mass fraction of $MgCl_2$ and $CaCl_2$ in the volatiles are analyzed. The results indicate that the volatilization loss of $MgCl_2$ is less than 2.5%, and that of $CaCl_2$ is below 1% in all cases. Due to the limited amount, $CaCl_2$ in the volatiles is difficult to detect by XRD. Additionally, the addition of $CaCl_2$ can further reduce the volatilization loss of $MgCl_2$. Therefore, the volatilization of either $MgCl_2$ or $CaCl_2$ would not cause significant problems for the chlorination of $ZnFe_2O_4$.

Figure 13 shows XRD patterns and Raman spectra of Solids-R (insoluble phases in residues in the crucible) after reacting $ZnFe_2O_4$ with different $MgCl_2$–$CaCl_2$ mixtures for

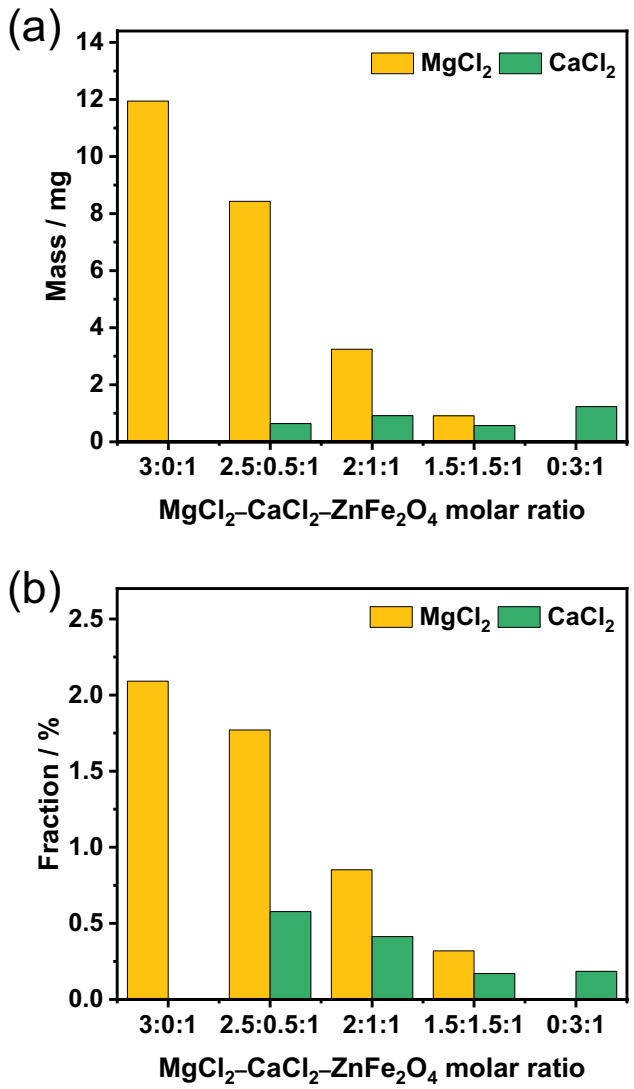

Fig. 12 **a** The mass of $MgCl_2$ and $CaCl_2$ in the volatiles, and **b** the mass fraction of $MgCl_2$ and $CaCl_2$ in the volatiles relative to the initial amount in the reactant after reaction at 950 °C for 120 min in Ar

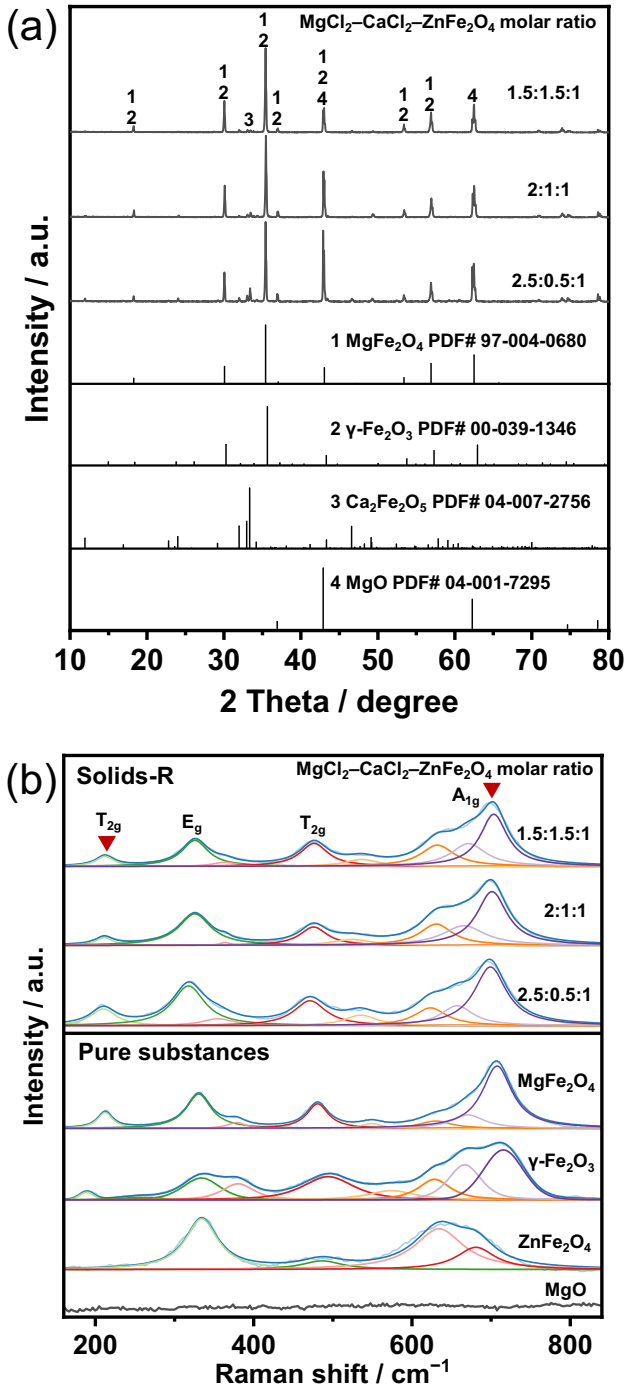

Fig. 13 **a** XRD patterns and **b** Raman spectra of Solids-R (insoluble phases in residues in the crucible) after reacting $ZnFe_2O_4$ with different $MgCl_2$–$CaCl_2$ mixtures for 120 min at 950 °C in Ar

120 min at 950 °C in Ar. Diffraction peaks belonging to a spinel phase and MgO are clearly observed in the XRD pattern. $Ca_2Fe_2O_5$ can also be detected, although the diffraction peaks are weak. The obtained Raman spectra have been deconvoluted into individual Lorentzian peaks for analysis. The peak of T_{2g} mode at ~ 210 cm^{-1} and the peak of A_{1g} mode at ~ 700 cm^{-1} indicate the occupation of Mg^{2+} in the octahedral and tetrahedral sites in the spinel structure [45, 46]. Thus, we infer that the spinel phase in Solids-R should be $MgFe_2O_4$ rather than $ZnFe_2O_4$ or Fe_2O_3. Figure 14 shows the SEM image and EDS mapping results of Solids-R (insoluble phases in residues in the crucible) after reacting $ZnFe_2O_4$ with $MgCl_2$–$CaCl_2$ mixtures for 120 min at 950 °C in Ar. Phases with compositions close to that of $MgFe_2O_4$ (Point A) and MgO (Point B) can be observed.

We also notice that with the increase in $CaCl_2$ addition, more $MgFe_2O_4$ is generated. These results suggest that the addition of $CaCl_2$ leads to the formation of $MgFe_2O_4$ and $Ca_2Fe_2O_5$, which inhibit the chlorination of Fe.

It is considered that $CaCl_2$ in $MgCl_2$ influences the reaction with $ZnFe_2O_4$ from two aspects. At first, since $CaCl_2$

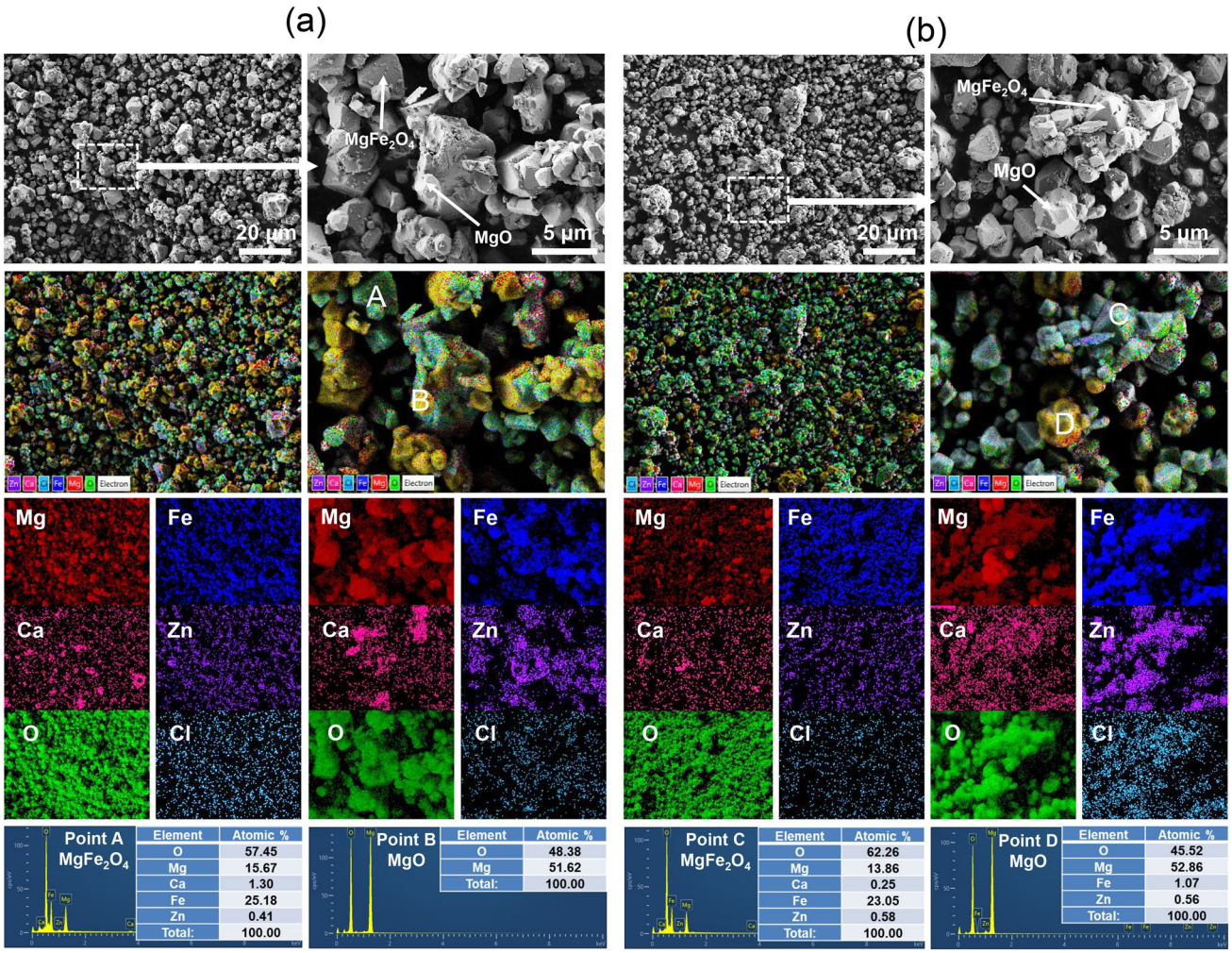

Fig. 14 SEM image and EDS mapping results of Solids-R (insoluble phases in residues in the crucible) after reacting $MgCl_2$–$CaCl_2$–$ZnFe_2O_4$ [molar ratios are **a** 2.5:0.5:1 and **b** 1.5:1.5:1] for 120 min at 950 °C in Ar

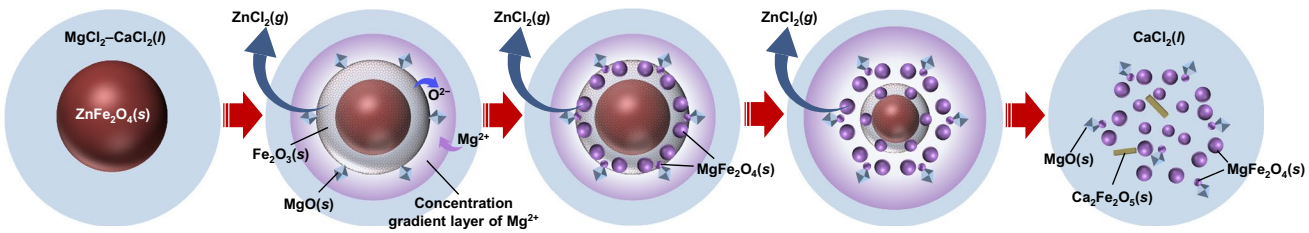

Fig. 15 Schematic representation of the reaction mechanism between solid $ZnFe_2O_4$ and molten $MgCl_2$–$CaCl_2$

and $MgCl_2$ are perfectly miscible, the addition of $CaCl_2$ is equivalent to lowering the concentration and thermodynamic activity of $MgCl_2$. Assuming reactions (2) and (3) are one-order reactions, the forward reaction rate (r) can be written as $r = k[MgCl_2]$, where k is the rate constant and $[MgCl_2]$ is the concentration of $MgCl_2$. As the equation shows, a decrease in the concentration of $MgCl_2$ will slow the reaction. On the other hand, the mobility of O^{2-} in the molten salt may rise with the increase in $CaCl_2$ content. Figure 15 illustrates the mechanism. Solid $ZnFe_2O_4$ first reacts with $MgCl_2$ in the $MgCl_2$–$CaCl_2$ mixture to produce $ZnCl_2$, MgO, and Fe_2O_3. A concentration gradient layer of $MgCl_2$ from the interface to the bulk will form because of the fast consumption of $MgCl_2$. Deficiency of $MgCl_2$ at the interface

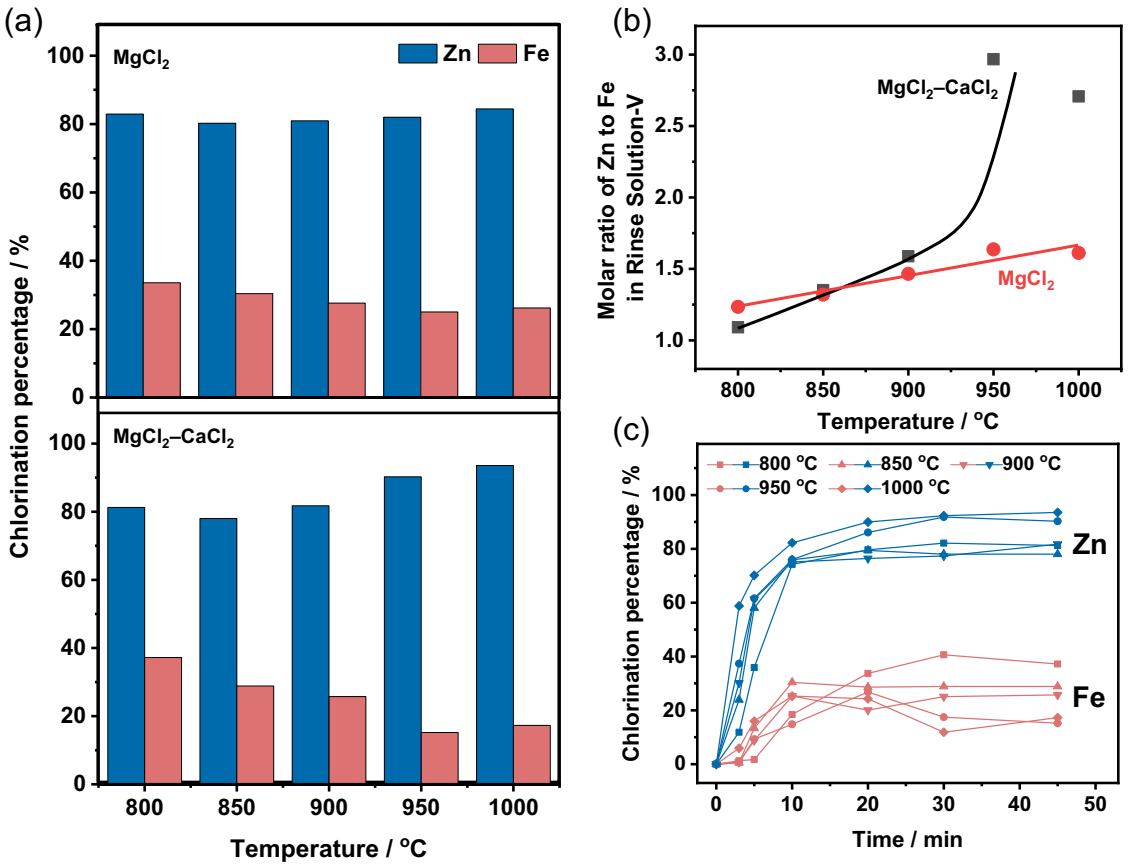

Fig. 16 Reaction between $ZnFe_2O_4$ and $MgCl_2$ ($MgCl_2$–$ZnFe_2O_4$ molar ratio = 3:1) or $MgCl_2$–$CaCl_2$ mixture ($MgCl_2$–$CaCl_2$–$ZnFe_2O_4$ molar ratio = 2.5:0.5:1) at different temperatures in Ar. **a** Chlorination percentages of Zn and Fe, **b** molar ratios of Zn to Fe in Rinse Solution-V (containing soluble phases in volatiles) after reaction for 120 min; **c** variation of chlorination percentages of Zn and Fe during the reactions between $ZnFe_2O_4$ and $MgCl_2$–$CaCl_2$ mixture ($MgCl_2$–$CaCl_2$–$ZnFe_2O_4$ molar ratio = 2.5:0.5:1) in 45 min

favors the reaction between $ZnFe_2O_4$ and $CaCl_2$ to produce mobile O^{2-}. Since the diffusion of $MgCl_2$ from the bulk to the interface promptly refill the deficiency, O^{2-} and Mg^{2+} turn Fe_2O_3 into more stable $MgFe_2O_4$ via reaction (8). When most $MgCl_2$ is consumed, a tiny amount of $CaFe_2O_5$ is also formed via reaction (7). MgO, $MgFe_2O_4$, and $Ca_2Fe_2O_5$ are the solid phases remaining in the system after sufficient reaction. As a result, chlorination of Fe is inhibited, and the selectivity of Zn chlorination is improved.

Synergistic Effect of Temperature and Adding $CaCl_2$

Figure 16a shows the chlorination percentages of Zn and Fe after the reactions between $ZnFe_2O_4$ and $MgCl_2$ or $MgCl_2$–$CaCl_2$ mixture for 45 min in Ar at different temperatures. When using $MgCl_2$ only ($MgCl_2$–$ZnFe_2O_4$ molar ratio = 3:1), the chlorination percentage of Zn is mainly independent of temperature, while that of Fe decreases slightly as the temperature increases. In the case of using $MgCl_2$–$CaCl_2$ mixture ($MgCl_2$–$CaCl_2$–$ZnFe_2O_4$ molar ratio = 2.5:0.5:1), the chlorination percentage of Zn increases from 81 to 94%, and that of Fe decreases from 38 to 15%, as the temperature increases from 800 to 1000 °C. These results indicate that it becomes more effective to promote the selectivity of chlorinating Zn by increasing temperature after adding $CaCl_2$ in $MgCl_2$. Molar ratios of Zn to Fe in Rinse Solution-V in the case of using $MgCl_2$–$CaCl_2$ mixture at 950 °C and 1000 °C are larger than the values using $MgCl_2$ only (Fig. 16b). Figure 16c shows the variation of chlorination percentages of Zn and Fe during the reactions between $ZnFe_2O_4$ and $MgCl_2$–$CaCl_2$ mixtures ($MgCl_2$–$CaCl_2$–$ZnFe_2O_4$ molar ratio = 2.5:0.5:1) at different temperatures in Ar. A higher temperature favors the chlorination of Zn in terms of amount and rate, while the dependency of the chlorination rate of Fe on temperature is not apparent. Furthermore, the chlorination percentages of Fe exhibit fluctuations that are particularly pronounced at higher temperatures. Our previous study [41] suggested that these fluctuations may be attributed to the formation of insoluble FeOCl from $FeCl_x$ in the volatiles at elevated temperatures. This reaction may also facilitate the separation of Zn and Fe. Based on the selectivity and rate

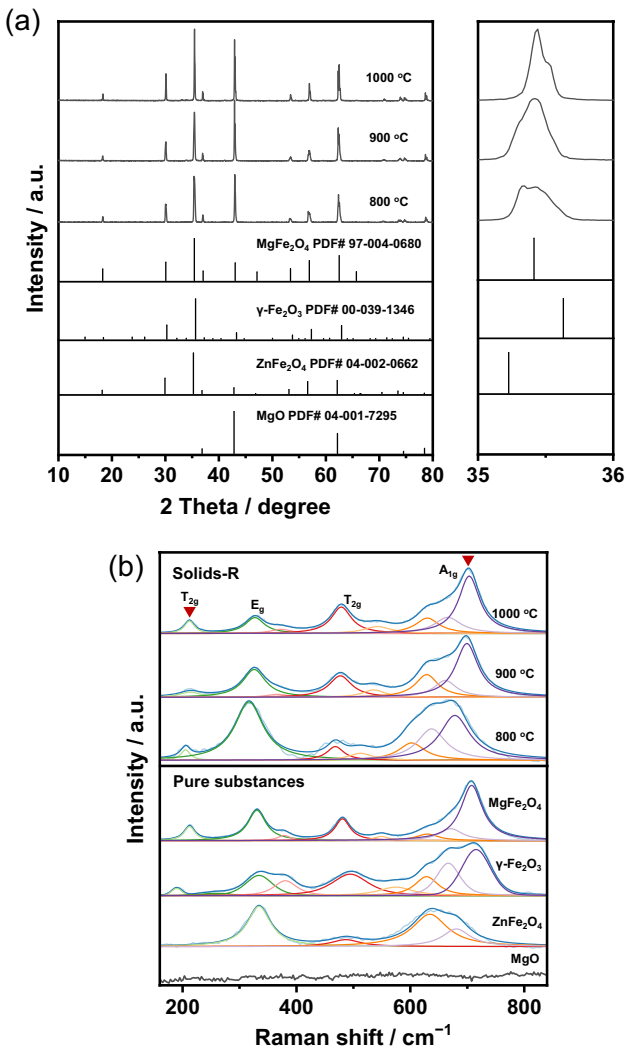

Fig. 17 **a** XRD patterns and **b** Raman spectra of Solids-R (insoluble phases in residues in the crucible) after reacting $ZnFe_2O_4$ with $MgCl_2$–$CaCl_2$ mixtures ($MgCl_2$–$CaCl_2$–$ZnFe_2O_4$ molar ratio = 2.5:0.5:1) at different temperatures for 45 min in Ar

of chlorination, the ideal temperature for chlorination is 950 °C when using the $MgCl_2$–$CaCl_2$ mixture.

Figure 17 shows the XRD patterns and Raman spectra of Solids-R (insoluble phases in residues in crucible) after reacting $ZnFe_2O_4$ with $MgCl_2$–$CaCl_2$ mixture ($MgCl_2$–$CaCl_2$–$ZnFe_2O_4$ molar ratio = 2.5:0.5:1) at different temperatures for 45 min in Ar. In all cases, formation of $MgFe_2O_4$ can be confirmed. As can be noticed, the diffraction peaks at 35.4° belonging to $MgFe_2O_4$ and the Raman spectra peak of A_{1g} mode at ~ 700 cm^{-1} are significantly intensified as temperature increases. This trend indicates that a higher temperature promotes the formation of $MgFe_2O_4$.

The formation of $MgFe_2O_4$ from Fe_2O_3 can be expressed by reaction (8). The formation rate can be written as $r = k[Mg^{2+}][O^{2-}]$. The rate constant k would increase with temperature, and the concentration of O^{2-} ($[O^{2-}]$) will also rise due to the increase in solubility. Therefore, the formation rate of $MgFe_2O_4$ increases with the temperature. Fast conversion of Fe_2O_3 into more stable phases, such as $MgFe_2O_4$, in molten $MgCl_2$–$CaCl_2$ at higher temperatures could explain why the chlorination of Fe is precluded.

Conclusions

This work clarifies the distinct reaction behavior of $ZnFe_2O_4$ between using $MgCl_2$ and using $CaCl_2$. Although $MgCl_2$ is a more powerful chlorinating agent, the capability of separating Zn and Fe is not as good as that of $CaCl_2$. Fast and selective chlorination of Zn from $ZnFe_2O_4$ happens by reacting $ZnFe_2O_4$ and $MgCl_2$–$CaCl_2$ mixture. By raising the mobility of O^{2-} in the molten salt, $CaCl_2$ facilitates the formation of stable Fe-bearing phases such as $MgFe_2O_4$ and $Ca_2Fe_2O_5$, thereby inhibiting the chlorination of Fe. Moreover, it becomes more effective in promoting the selectivity of chlorinating Zn by increasing temperature after adding $CaCl_2$ in $MgCl_2$. These results demonstrate the prospect of efficient separation of Zn from $ZnFe_2O_4$ by reaction with molten $MgCl_2$–$CaCl_2$ mixture.

Acknowledgements The authors thank Dr. Yinjuan Chen and Mr. Ke Wang of Instrumentation and Service Center for Molecular Sciences at Westlake University for the assistance in the ICP-MS measurement and thank Ms. Ying Zhong and Dr. Xiaohe Miao of Instrumentation and Service Center for Physical Sciences at Westlake University for the XRD measurement.

Declarations

Conflict of interest On behalf of all authors, the corresponding author states that there is no conflict of interest.

References

1. Rostek L, Espinoza LT, Goldmann D, Loibl A (2022) A dynamic material flow analysis of the global anthropogenic zinc cycle: providing a quantitative basis for circularity discussions. Resour Conserv Recy 180:106154
2. Ye Q, Li G, Peng Z, Augustine R, Pérez MD, Liu Y, Liu M, Rao M, Zhang Y, Jiang T (2020) Microwave-assisted self-reduction of EAF dust-biochar composite briquettes for production of direct reduced iron. Powder Technol 362:781–789
3. U.S. Geological Survey (2022) Mineral commodity summaries. U.S. Geological Survey, Washington
4. Havlík T, e Souza BV, Bernardes AM, Schneider IAH, Miškufová A (2006) Hydrometallurgical processing of carbon steel EAF dust. J Hazard Mater 135:311–318
5. Wu C, Chang F, Chen W, Tsai M, Wang Y (2014) Reduction behavior of zinc ferrite in EAF-dust recycling with CO gas as a reducing agent. J Environ Manag 143:208–213

6. Halli P, Agarwal V, Partinen J, Lundström M (2020) Recovery of Pb and Zn from a citrate leach liquor of a roasted EAF dust using precipitation and solvent extraction. Sep Purif Technol 236:116264
7. Halli P, Hamuyuni J, Leikola M, Lundström M (2018) Developing a sustainable solution for recycling electric arc furnace dust via organic acid leaching. Miner Eng 124:1–9
8. Kerry T, Peters A, Georgakopoulos E, Dugulan I, Meijer K, Hage J, Offerman E, Yang Y (2022) Zinc vaporization and self-reduction behavior of industrial waste residues for recycling to the HIsarna furnace. J Sustain Metall 8:658–672
9. Omran M, Fabritius T, Heikkinen E-P (2019) Selective zinc removal from electric arc furnace (EAF) dust by using microwave heating. J Sustain Metall 5:331–340
10. Tang H, Peng Z, Wang L, Anzulevich A, Rao M, Li G (2023) Direct conversion of electric arc furnace dust to zinc ferrite by roasting: effect of roasting temperature. J Sustain Metall 9:1–12
11. Van Winkel S, Scheunis L, Verhaeghe F, Blanpain B, Malfliet A (2019) Chlorine addition to existing zinc fuming processes: a thermodynamic study. J Sustain Metall 5:538–550
12. Wang L, Peng Z, Lin X, Ye Q, Ye L, Zhang J, Liu Y, Liu M, Rao M, Li G (2021) Microwave-intensified treatment of low-zinc EAF dust: a route toward high-grade metallized product with a focus on multiple elements. Powder Technol 383:509–521
13. Ye Q, Peng Z, Li G, Lee J, Liu Y, Liu M, Wang L, Rao M, Zhang Y, Jiang T (2019) Microwave-assisted reduction of electric arc furnace dust with biochar: an examination of transition of heating mechanism. ACS Sustain Chem Eng 7:9515–9524
14. Zhang D, Ling H, Yang T, Liu W, Chen L (2019) Selective leaching of zinc from electric arc furnace dust by a hydrothermal reduction method in a sodium hydroxide system. J Clean Prod 224:536–544
15. Wang J, Zhang Y, Cui K, Fu T, Gao J, Hussain S, AlGarni TS (2021) Pyrometallurgical recovery of zinc and valuable metals from electric arc furnace dust—a review. J Clean Prod 298:126788
16. Pickles C (2008) Thermodynamic analysis of the selective carbothermic reduction of electric arc furnace dust. J Hazard Mater 150:265–278
17. Chairaksa-Fujimoto R, Inoue Y, Umeda N, Itoh S, Nagasaka T (2015) New pyrometallurgical process of EAF dust treatment with CaO addition. Int J Min Met Mater 22:788–797
18. Chairaksa-Fujimoto R, Maruyama K, Miki T, Nagasaka T (2016) The selective alkaline leaching of zinc oxide from Electric Arc Furnace dust pre-treated with calcium oxide. Hydrometallurgy 159:120–125
19. Miki T, Chairaksa-Fujimoto R, Maruyama K, Nagasaka T (2016) Hydrometallurgical extraction of zinc from CaO treated EAF dust in ammonium chloride solution. J Hazard Mater 302:90–96
20. Gaballah I, Djona M, Mugica J, Solozobal R (1994) Valuable metals recovery from spent catalysts by selective chlorination. Resour Conserv Recy 10:87–96
21. Pickles C (2009) Thermodynamic analysis of the selective chlorination of electric arc furnace dust. J Hazard Mater 166:1030–1042
22. Hu X, Jiang P, Yan Z, Zhu L, Chou K-C, Matsuura H, Tsukihashi F (2013) Selective chlorination reaction of Cu_2O and FeO mixture by $CaCl_2$. ISIJ Int 53:541–543
23. Ma Y, Zhou X, Tang J, Liu X, Gan H, Yang J (2021) One-step selective recovery and cyclic utilization of valuable metals from spent lithium-ion batteries via low-temperature chlorination pyrolysis. Resour Conserv Recy 175:105840
24. Huang Y, Shao P, Yang L, Zheng Y, Sun Z, Fang L, Lv W, Yao Z, Wang L, Luo X (2021) Thermochemically driven crystal phase transfer via chlorination roasting toward the selective extraction of lithium from spent $LiNi_{1/3}Co_{1/3}Mn_{1/3}O_2$. Resour Conserv Recy 174:105757
25. Xing Z, Cheng G, Yang H, Xue X, Jiang P (2020) Mechanism and application of the ore with chlorination treatment: a review. Miner Eng 154:106404
26. Matsuura H, Hamano T, Tsukihashi F (2006) Chlorination kinetics of $ZnFe_2O_4$ with Ar-Cl_2-O_2 gas. Mater Trans 47:2524–2532
27. Matsuura H, Hamano T, Tsukihashi F (2006) Removal of Zn and Pb from Fe_2O_3–$ZnFe_2O_4$–ZnO–PbO mixture by selective chlorination and evaporation reactions. ISIJ Int 46:1113–1119
28. Matsuura H, Tsukihashi F (2006) Chlorination kinetics of ZnO with Ar-Cl_2-O_2 gas and the effect of oxychloride formation. Metall Mater Trans B 37:413–420
29. Al-Harahsheh M (2018) Thermodynamic analysis on the thermal treatment of electric arc furnace dust-PVC blends. Arab J Sci Eng 43:5757–5769
30. Al-Harahsheh M, Al-Nu'airat J, Al-Otoom A, Al-jabali H, Al-zoubi M (2019) Treatments of electric arc furnace dust and halogenated plastic wastes: a review. J Environ Chem Eng 7:102856
31. Al-Harahsheh M, Al-Otoom A, Al-Jarrah M, Altarawneh M, Kingman S (2018) Thermal analysis on the pyrolysis of tetrabromobisphenol A and electric arc furnace dust mixtures. Metall Mater Trans B 49:45–60
32. Al-Harahsheh M, Kingman S, Al-Makhadmah L, Hamilton IE (2014) Microwave treatment of electric arc furnace dust with PVC: dielectric characterization and pyrolysis-leaching. J Hazard Mater 274:87–97
33. Altarawneh S, Al-Harahsheh M, Dodds C, Buttress A, Kingman S (2022) Thermal degradation kinetics of polyvinyl chloride in presence of zinc oxide. Thermochim Acta 707:179105
34. Lee GS, Song YJ (2007) Recycling EAF dust by heat treatment with PVC. Miner Eng 20:739–746
35. Iwase G, Okumura K (2021) Nonisothermal investigation of reaction kinetics between electric arc furnace dust and calcium chloride under carbon-containing conditions. ISIJ Int 61:2483–2489
36. Sato H, Okumura K (2020) Recovery of zinc by reaction between electric arc furnace dust and calcium chloride. Tetsu to Hagane 106:82–90
37. Guo T, Hu X, Hou X, Matsuura H, Tsukihashi F, Zhou G (2011) Chlorination reaction mechanism between $ZnFe_2O_4$ and $CaCl_2$. J Univ Sci Technol Beijing 33:474
38. Guo T, Hu X, Shu Q, Zhou G (2008) Removal of zinc from $ZnFe_2O_4$ by selective chlorination and evaporation. J Chin Rare Earth Soc 26:849–853
39. Cooper EI, Kohn DH (1983) The use of molten magnesium chloride in the preparation of crystalline ceramic powders. Ceram Int 9:68–72
40. Kang J, Okabe TH (2013) Removal of iron from titanium ore through selective chlorination using magnesium chloride. Mater Trans 54:1444–1453
41. Huang J, Sohn I, Kang Y, Yang X (2022) Separation of Zn and Fe in $ZnFe_2O_4$ by reaction with $MgCl_2$. Metall Mater Trans B 53:2634–2646
42. Wenz DA, Johnson I, Wolson RD (1969) $CaCl_2$-rich region of the $CaCl_2$-CaF_2-CaO system. J Chem Eng Data 14:250–252
43. Guo T, Hu X, Matsuura H, Tsukihashi F, Zhou G (2010) Kinetics of Zn removal from ZnO–Fe_2O_3–$CaCl_2$ System. ISIJ Int 50:1084–1088
44. Ito M, Morita K (2004) The solubility of MgO in molten $MgCl_2$-$CaCl_2$ salt. Mater Trans 45:2712–2718
45. Murugesan C, Okrasa L, Ugendar K, Chandrasekaran G, Liu X, Diao D, Shen J (2022) Improved magnetic and electrical properties of Zn substituted nanocrystalline $MgFe_2O_4$ ferrite. J Magn Magn Mater 550:169066
46. Da Silva S, Nakagomi F, Silva M, Franco A, Garg V, Oliveira A, Morais P (2012) Raman study of cations' distribution in $Zn_xMg_{1-x}Fe_2O_4$ nanoparticles. J Nanopart Res 14:1–10

Publisher's Note Springer Nature remains neutral with regard to jurisdictional claims in published maps and institutional affiliations.

Springer Nature or its licensor (e.g. a society or other partner) holds exclusive rights to this article under a publishing agreement with the author(s) or other rightsholder(s); author self-archiving of the accepted manuscript version of this article is solely governed by the terms of such publishing agreement and applicable law.

Authors and Affiliations

Jingdong Huang[1,2] · Guangqiang Li[3] · Xiao Yang[2]

✉ Guangqiang Li
liguangqiang@wust.edu.cn

✉ Xiao Yang
yangxiao@westlake.edu.cn

[1] School of Materials Science and Engineering, Zhejiang University, Hangzhou 310027, Zhejiang, China

[2] Key Laboratory of Coastal Environment and Resources of Zhejiang Province, School of Engineering, Westlake University, 600 Dunyu Road, Hangzhou 310030, Zhejiang, China

[3] Key Laboratory for Ferrous Metallurgy and Resources Utilization of Ministry of Education, Wuhan University of Science and Technology, Wuhan 430081, Hubei, China